Chapter V

Analysis of Experimental Results:

5.1 Introduction:

The results obtained from the various experimental data presented in chapter IV are analyzed in this chapter. For clarity, this chapter is divided into three major sections. The electrical and optical measurements of both crystalline germanium and crystalline silicon are analyzed in section 5.2. The results of the optical characterization of a-Si:H are analyzed in section 5.3. The effects of annealing on various parameters derived from the optical transmission spectrum of the film are discussed. From these results, the effect of hydrogen content on the thickness, refractive index and optical energy gap are studied and analyzed. Finally the results of the electrical characterization of a-Si:H are analyzed in section 5.4. In this section, the variation of conductivity, activation energy with annealing is studied. A correlation between the hydrogen content and the density of states at the Fermi level is discussed in this section.

5.2 Analysis of Crystalline semiconductors:-

5.2.1 Crystalline Germanium:-

The X-ray diffractogram of crystalline germanium is presented in figure 5.1. The diffractogram exhibits a sharp peak at 2θ equal to 28.39°, which correspond to the diffraction from <111> plane. The maximum intensity of the peak as observed in the diffractogram corresponds to Bragg reflected spectra of a certain order. Using Bragg's law $2d\sin\theta = n\lambda$, the lattice spacing of the crystalline germanium has been

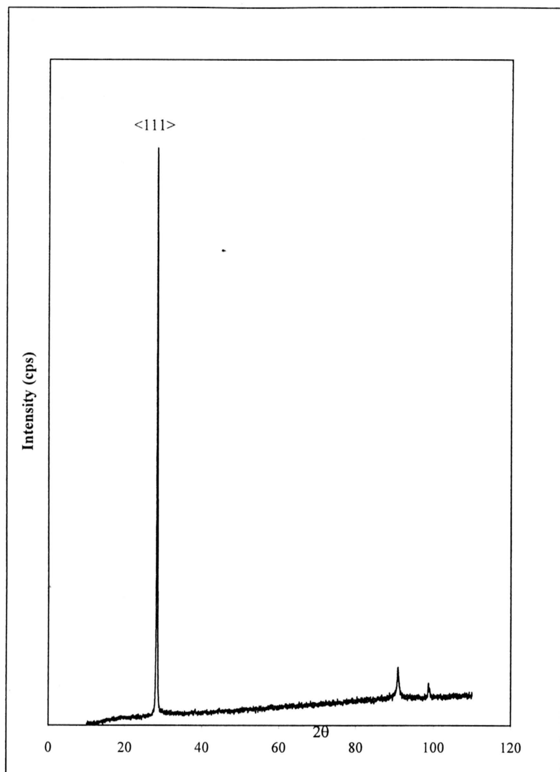

Figure 5.1 The X-ray Diffractogram of crystalline Germanium

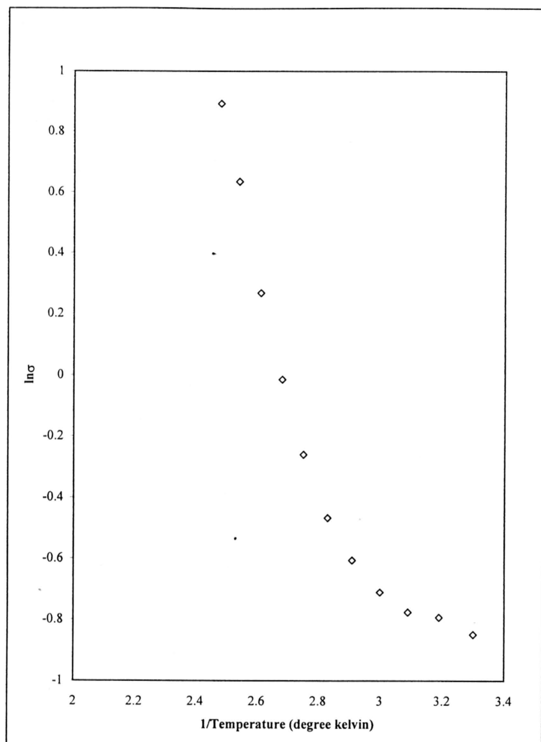

Figure 5.2 The variation of lnσ with Temperature Inverse for crystalline Germanium

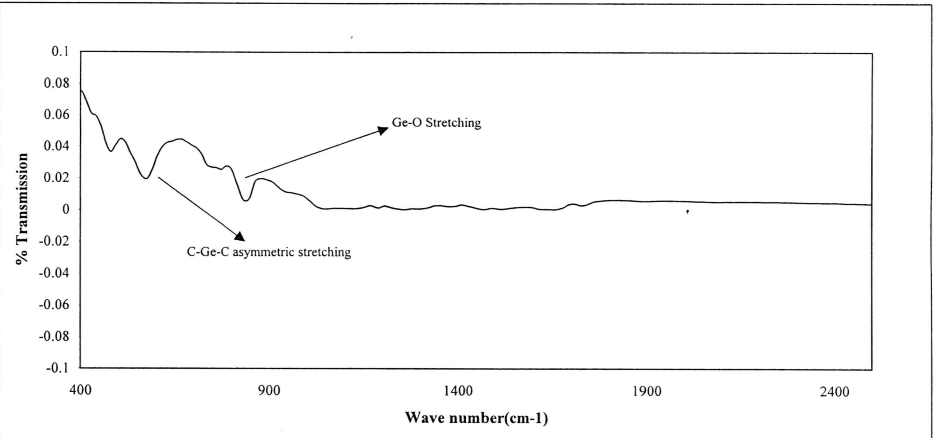

Figure 5.3 The Transmission spectrum of crystalline Germanium in the Infrared region.

determined to be equal to 6.29 $\mathring{A}$. The Bragg's law reported lattice spacing for Ge is quoted to be 5.64 $\mathring{A}$ for this plane [74]. The difference in value is probably due to the strained lattice structure of this crystalline germanium sample.

The lnσ versus 1/T plot of crystalline germanium is presented in figure 5.2 where σ is the conductivity and T is the measured temperature in Kelvin. From the linear part of the graph of lnσ versus 1/T at higher temperatures, the slope $\frac{E_g}{2k}$, as discussed in the theory of crystalline semiconductors (Chapter II) was calculated. Thus, the value for E_g is determined to be equal to 0.65eV, which is in agreement with the reported value of energy gap of crystal Ge, which at 300°k is equal to 0.66eV [74]. The conductivity of crystal Ge at room temperature is found to be equal to $4.2\times10^{-1}\Omega^{-1}cm^{-1}$.

The FTIR spectrum of crystalline Germanium is presented in figure 5.3. The sample exhibits two absorption bands in the transmission spectrum at wave number $575cm^{-1}$ and $850cm^{-1}$. These bands are respectively assigned to be C-Ge-C asymmetric stretching [58,59] and Ge-O stretching [58,60,61,75,76] bonding configurations. From the spectral analysis it is evident that crystalline Germanium has carbon and oxygen contamination.

5.2.2 Crystalline Silicon:-

The X-ray diffractogram of crystalline silicon presented in figure 5.4 shows a sharp peak at 2θ equal to 69.53°, corresponding to diffraction from <111> plane at lattice

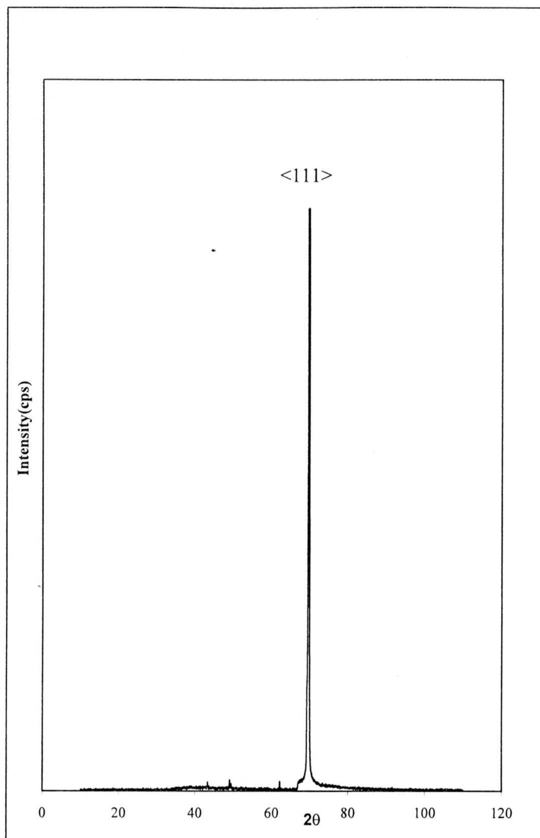

Figure 5.4 The X-ray diffractogram of crystal Silicon

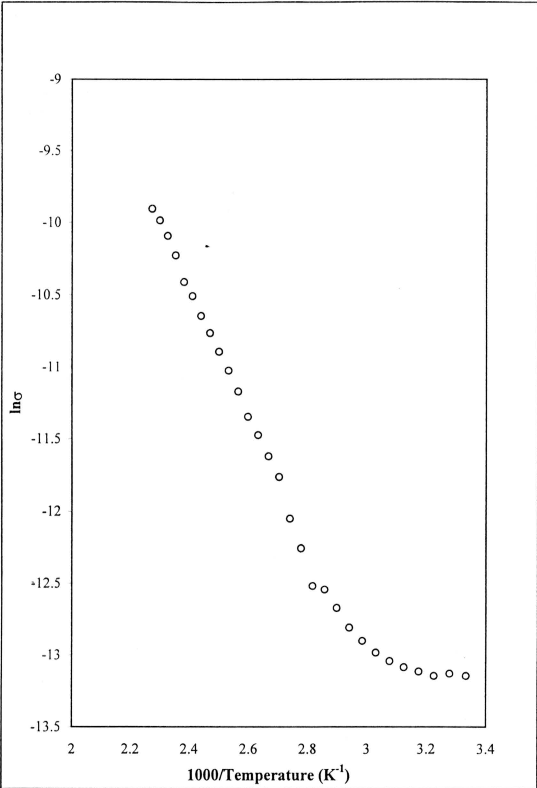

Figure 5.5 The variation of ln conductivity against Temperature Inverse for crystalline Silicon

spacing of 5.43 Å as calculated using the Bragg's law. Reported lattice spacing for crystalline silicon is quoted to be at 5.43 Å [74] for this plane. The experimental results are in good agreement with the reported value showing that the crystal is a perfect one.

The lnσ versus 1/T plot of crystalline silicon is presented in figure 5.5, where σ is

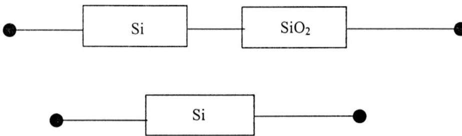

Figure 5.6(a) A block diagram of the formation of Oxide layer on top of Crystal Si.

the conductivity ($\Omega^{-1}cm^{-1}$) and T is the temperature (°K). From the graph the activation energy or the energy gap of the sample was calculated as discussed in the theory of crystalline semiconductors in chapter II. The crystalline silicon used in this work is industrially prepared and n-type. The activation energy of this silicon was found to be 0.72eV only while the accepted value is 1.12eV [74]. The conductivity of crystalline silicon at room temperature was found to be $0.5\times10^{-5}\Omega^{-1}cm^{-1}$.This discrepancy in the result can be explained by presuming that a layer of SiO_2 grows on the top of Si sample. The SiO_2 absorption band in the FTIR spectrum of crystalline silicon shown in figure 5.7 further emphasizes the contamination of the sample with oxide layer. A simple model presumed above is represented in figure 5.6(a). It explains the lower conductivity due to oxidation. For pure silicon the conductivity increases monotonically with increase in temperature. But if a layer of

SiO_2 is imagined to be in series with silicon, as represented in figure 5.6(a), the former would behave as an ordinary resistance and in that case the conductivity of Silicon +SiO_2 would be a little lower than the expected value, as explained in Figure 5.6(b).

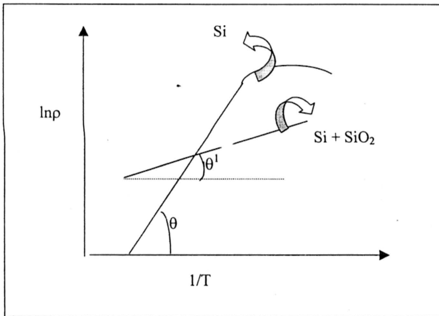

Figure 5.6(b) The variation of lnρ verses 1/T for pure Si and Si + SiO_2 sample.

The Transmission Spectroscopy of crystalline silicon was measured in the infrared and ultraviolet visible regions of the electromagnetic spectrum. The FTIR spectrum of crystalline silicon is shown in figure 5.7. The spectrum exhibits two absorption bands at $611cm^{-1}$ and at $1125cm^{-1}$. The observed bands are respectively assigned to be due to Si-H wagging [62-64] and SiO_2 out of phase stretching bond [65]. The spectral analysis reveals the oxygen and hydrogen intrinsic contamination of the sample during the growth of the crystal.

The UV-VIS transmission spectrum of crystalline silicon has already been given in figure 4.15. From the data of the transmission spectrum, the absorption coefficient α

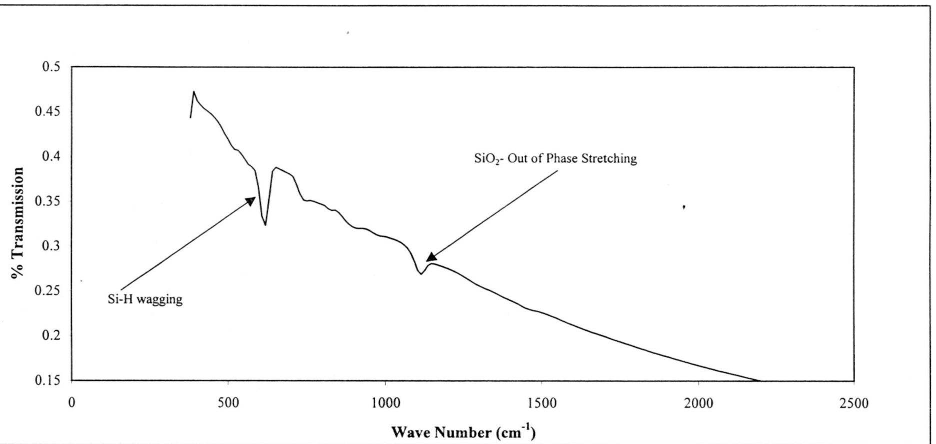

Figure 5.7 The Transmission spectrum of Silicon in the Infrared region.

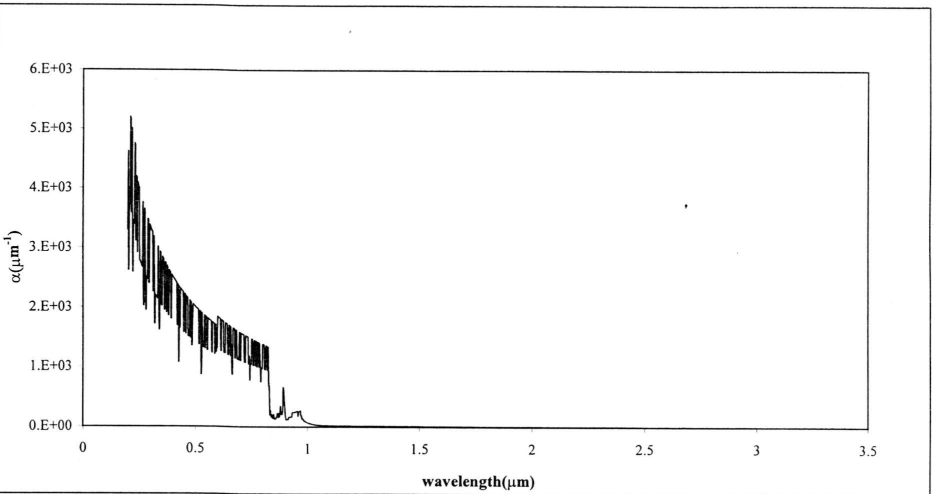

Figure 5.8 The variation of optical absorption coefficient with wavelength for crystalline Silicon.

(μm^{-1}) was calculated using the expression 2.9, which is given by $\alpha = \frac{4 \pi k}{\lambda}$ while k is calculated using the expression (2.8) which is given as $R = \frac{(1-n)^2 + k^2}{(1+n)^2 + k^2}$. Figure 5.8 represents the variation of the absorption coefficient (α) of crystalline silicon with wavelength (λ) in the range of 0.2µm-3µm. The actual calculation used to measure these parameters has already been explained in detail in chapter III. It is evident that absorption coefficient decreases with the wavelength and around 1.2µm α becomes zero, which correspond to the energy gap of the crystalline silicon. The energy gap was calculated using the expression [77],

$$E_g(eV) = \frac{1.24}{\lambda(\mu m)} \quad (5.1)$$

Using the above expression the energy gap of the crystal silicon was found to be equal to 1.03eV which is slightly lower than the quoted value of crystalline silicon [74] but was still within the experimental error range.

5.3 Analysis of Optical characterization results of Hydrogenated amorphous silicon:-

5.3.1 Effect of Annealing on Hydrogen content:-

In this work a-Si:H film is systematically annealed to provide information on hydrogen evolution steps as the annealing temperature is increased. Figure 5.9 shows the effect of annealing on the hydrogen content of the a-Si:H film studied. The figure shows that the hydrogen content decreases almost uniformly with the increase in annealing temperature when annealed above 100°C. Hydrogen evolution at low annealing temperature as observed in this sample indicates the presence of weakly bonded hydrogen in the form of multiply grouped polyhydride bonds (SiH_2, $-SiH_3$

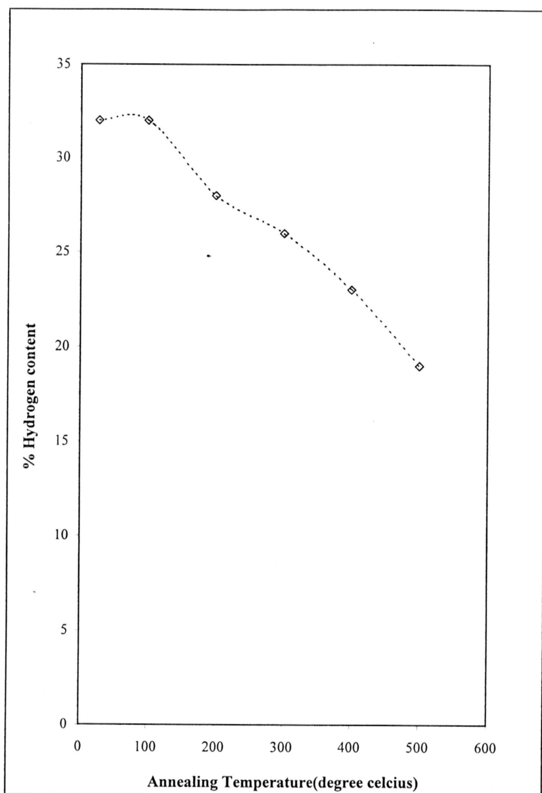

Figure 5.9 The variation of hydrogen content in a-Si:H on annealing.

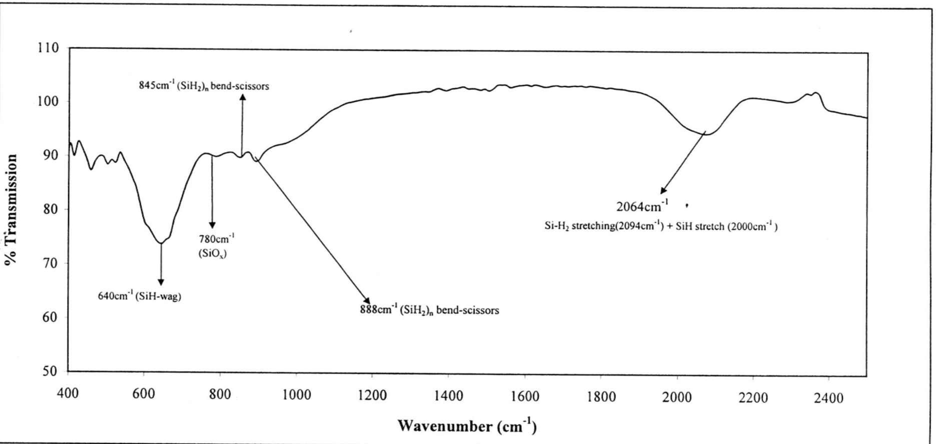

Figure 5.10 The Infrared Spectrum of a-Si:H

and $(SiH_2)_n$) [78] which is characteristic of a-Si:H films prepared at room temperature. The evolution of hydrogen at low annealing temperature is consistent with the fact that the sample was prepared at room temperature. The infrared spectrum of the film shown in figure 5.10 further confirms the presence of the polyhydride bonding sites in this film. The shift of the broad absorption band representing these bonding sites towards higher wave number ($2064cm^{-1}$) indicates the dominant presence of $(SiH_2)_n$ bonds in the film as compared to monohydride, Si-H bonds. Biegelsen et al [79] on the basis of hydrogen evolution and IR measurements on a-Si:H alloys suggest that peak evolution of hydrogen occurs at T_A<250°C from SiH_3, at 320°C from $(Si\text{-}H_2)_n$ at 420°C from near surface bonded Si-H and/ or Si-H_2 and at 600°C from bulk Si-H and Si-H_2 sites respectively. Thus results obtained from this work infer that when annealed at 200°C hydrogen from SiH_3 and $(SiH_2)_n$ bonding sites from or near the surface are evolved. The hydrogen content from these sites represent approximately 4% of the hydrogen content in the film (refer table 5.1). Further annealing at 300°C results in the evolution of hydrogen from bulk SiH_3 bonding sites. Approximately only 2% of the hydrogen in the film is bonded in this configuration in the bulk. Hydrogen from bulk $(Si\text{-}H)_n$ site is evolved when the sample is annealed at 400°C (~3%). Finally when annealed at 500°C, hydrogen is evolved from near surface bonded Si-H and/or Si-H_2 bonding sites leaving behind hydrogen bonded in the Si-H and Si-H_2 bonding configuration in the bulk of the film (~19%). Thus annealing of the a-Si:H studied in this work results in hydrogen being evolved from various bonding sites. The film is typical of a-Si:H film prepared at low substrate temperature since it contains weakly bonded polyhydride bonds. Hydrogen usually acts as Si-Si bond strain reliever and dangling bond terminator in a-Si:H network but excess hydrogen in the form of polyhydride

bonds forms columnar structure which induces more strain in the film. Annealing removes these hydrogen to form a more ordered Si-matrix.

5.3.2 Effect of Hydrogen Content on Thickness:

Figure 5.11 shows the effect of annealing on thickness of the film, while the effect of hydrogen content on thickness of the film is shown in figure 5.12. From figure 5.11 it is observed that with increase in annealing temperature the thickness decreases although a slight increase in thickness was observed when the sample was annealed at 300°C and 500°C. Generally the thickness of the film increases with hydrogen content. The hydrogen atoms incorporated into the a-Si matrix occupy space and thus increase the thickness of the film. Subsequent annealing of the film result in the evolution of hydrogen atoms from the various bonding configurations which results in a more compact and denser structure. From figure 5.12 it is observed that with the evolution of hydrogen atoms from the structure, the film thickness decreases except when the sample was annealed at 300°C and 500°C. This could be due to rearrangement of the structure due to annealing and failure of reconstruction of Si-Si bonds in the Si-matrix.

5.3.3 Effect of Hydrogen content on the Refractive index of the sample:-

Figure 5.13 shows the effect of hydrogen content on the refractive index of the sample. The figure shows that the refractive index decreases sharply with increase in hydrogen content when the hydrogen content is less than 25%. However, when the hydrogen content is above 25%, no significant variation is observed with further increase in the hydrogen content. This type of behaviour was also observed by other workers [80,81]. Thus, the refractive index decreases with the increase in hydrogen

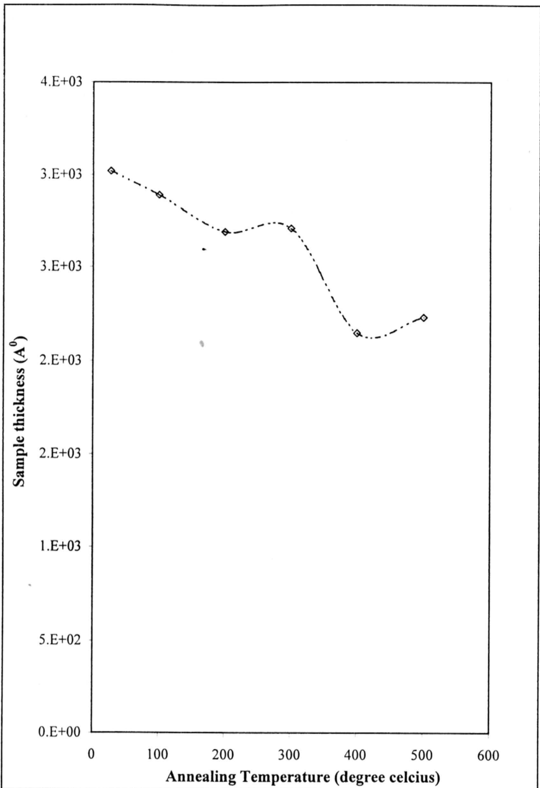

Figure 5.11 The variation of sample thickness with annealing temperature.

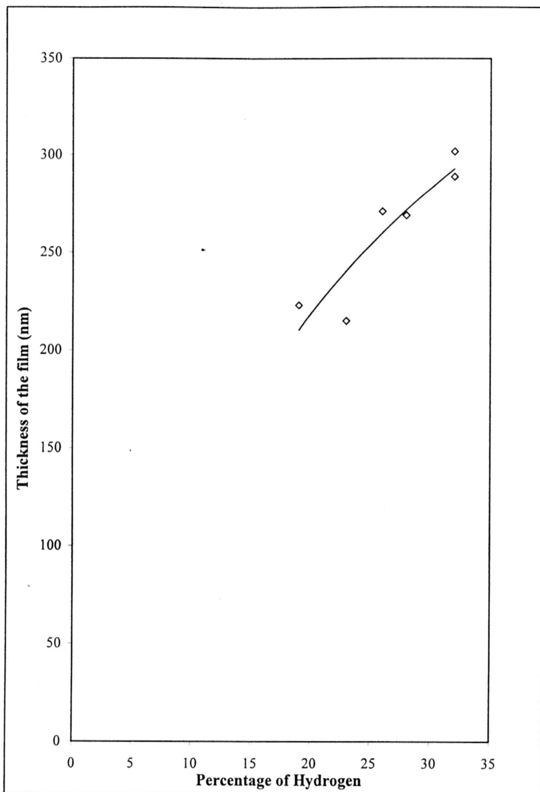

Figure 5.12 The Effect of Hydrogen content on the Thickness of the Film

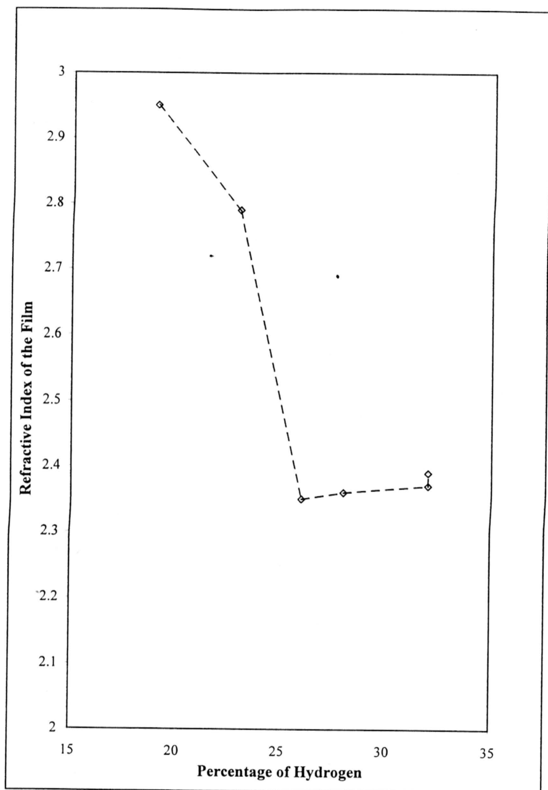

Figure 5.13 Effect of Hydrogen content on the Refractive index of the sample

content only when the hydrogen content is less than a certain percentage which is characteristic of the film.

5.3.4 Effect of Annealing Temperature on the Optical Energy gap:-

Figure 5.14 shows the effect of annealing on the optical gap, E_{opt} of the a-Si:H film studied. The optical energy gap values at various annealing temperatures studied are presented in table 5.1. As analyzed in section 5.3.1the a-Si:H film studied is saturated with hydrogen and annealing at low temperature (<300°C) results in hydrogen being evolved from weakly bonded SiH_3 and $(SiH_2)_n$ bonding sites at the surface and SiH_3 sites in the bulk. The optical energy gap in figure 5.14 increases slightly when annealed at 100°C due to thermal relaxation of the material [82] and remains constant (within experimental error) when annealed at 200°C and 300°C. A significant decrease in the optical gap results when the sample is annealed at 400°C and remain constant when annealed at 500°C. This variation in E_{opt} with annealing temperature is characteristic of a hydrogen saturated a-Si:H film [83]. Annealing reduces both the number and size of matrix defects and transforms some hydrogen dependent defect into pure matrix defects. A competition exists between the creation and annealing of pure Si matrix defects, which result in constant and slight decrease in hydrogen percentage during the initial stages of hydrogen evolution. The decrease in optical gap only occurs at high annealing temperature (400°C) when the transformation of hydrogen related defects into pure matrix defects is more dominant than the healing of pure matrix defects. The constant or slight decrease in the hydrogen percentage values when the sample is annealed at temperatures below 400°C also infer that hydrogen removed from SiH_3 (at the surface and in the bulk) and $(SiH_2)_n$ (at the surface) bonding sites only results in hydrogen related defects

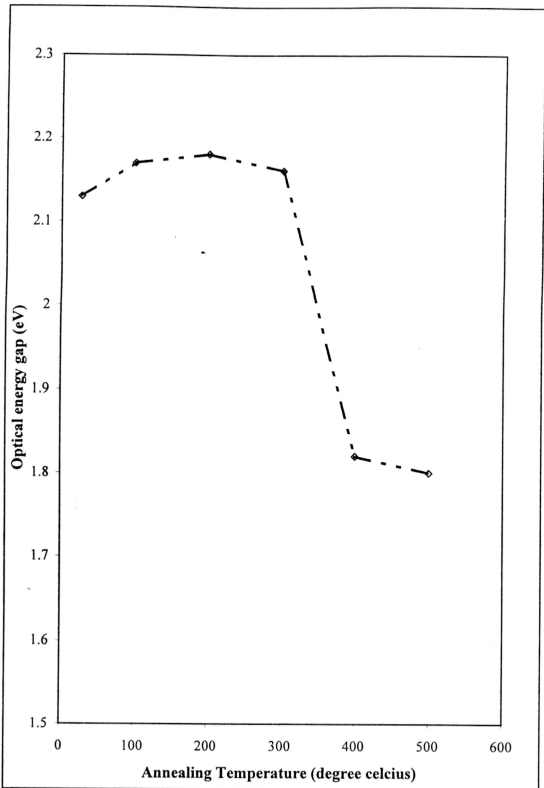

Figure 5.14 Effect of Annealing Temperature on the Optical energy gap of a-Si:H

(dangling bonds) which forms deep defect states at the mid gap. Hydrogen removed from $(SiH_2)_n$ sites in the bulk transforms hydrogen related defects states in the mid gap into shallow matrix defect states which decreases the optical energy gap (T_A=400°C). Annealing at 500°C results in hydrogen being removed from Si-H and Si-H_2 bonding sites at the surface. Hydrogen evolved from these bonding sites has no significant effect on the optical energy gap due to an equilibrium situation between healing of pure matrix defects by annealing (increase in E_{opt}) and transformation of hydrogen related defects into pure matrix defects (decrease in E_{opt}).

5.3.5 Effect of hydrogen content on the Optical energy gap:-

The basic role of hydrogen in a-Si:H is to satisfy the dangling bonds or cancellation of free spins. The hydrogen atoms incorporated in the a-Si network modify the silicon matrix, which control the optical gap [84]. The effect of hydrogen content on the optical gap of the sample is given in figure 5.15. Analysis of the figure reveals that the optical energy gap increased slightly or remained almost constant when the amount of hydrogen evolved from the sample was very low. The hydrogen lowers the number of dangling bonds and reduces the number of localized states in the gap [85]. The slight increase in the optical gap was the effect of annealing, which gave rise to deep states or dangling bonds in the middle of the gap and annealed the shallow defects. When the amount of hydrogen atoms present in the sample was reduced further, the optical gap decreased significantly. This significant decrease in E_{opt} indicated that the formation of dangling bond due to removal of sufficient hydrogen from the film resulted not only in deep defects but also matrix defects. From the discussion in previous section, this effect was due to hydrogen removed

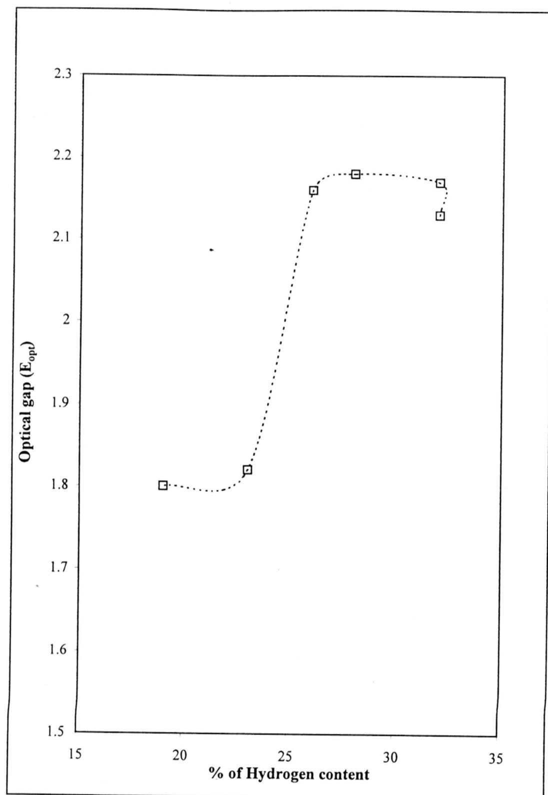

Figure 5.15 The variation of optical energy gap with hydrogen content.

from $(SiH_2)_n$ bonding sites in the bulk. Thus, it could be generalized that high concentration of hydrogen atoms produced hydrogen related defects like columnar structures in the film and removal of hydrogen atoms by annealing initially produced dangling bonds which formed localized states in the midgap. Excessive removal of hydrogen atoms produced shallow matrix defects, which reduced the optical gap. Thus optical gap is controlled by the concentration of hydrogen atoms incorporated in the film and the bonding configurations at which it is incorporated which would give different electronic states in the pseudogap [86,87]. The results suggest that quality of the film improved with a small addition of hydrogen and it deteriorated when the hydrogen content in the sample is high.

5.4 Analysis of Electrical Characterization Results of a-SiH:

5.4.1 Effect of annealing on the conductivity of a-Si:H

The conductivity of a-Si:H sample was measured in the temperature range of 77K-320K. The results show that the dark conductivity of the film decreased when sample was annealed at temperatures of 300°C and below. The film annealed at 300°C showed optimum conductivity and the defects effecting conductivity in the film was minimized. On annealing the sample at 400°C the concentration of dangling bonds in the film increased significantly due to excess evolution of hydrogen atoms from the film. High concentration of dangling bonds was transformed into shallow matrix defects. The decrease in the optical energy gap explains the significant increase in conductivity. Subsequent annealing of the film at 500°C produced a more ordered structure due to recrystallization of the film as evident from the X-ray diffractogram of a-Si:H (see fig 4.3 (a)). Hence a drop in conductivity was observed. Figure 5.16 also shows the effect of light and dark

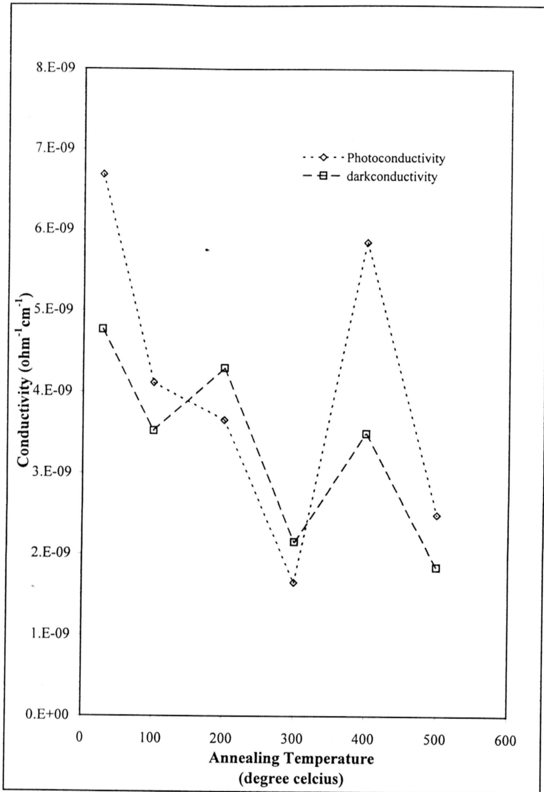

Figure 5.16 The variation of room temperature conductivity as a function of annealing temperature with and without background illumination.

conductivity at 300K for the as prepared and the sample annealed at 100°C, 200°C, 300°C, 400°C and 500°C. Photoconductivity is dominant in the as prepared film and the film annealed at 400°C. The film at these temperatures exhibited obvious difference between the light and dark conductivity. Defects and dangling bonds form localized energy states in forbidden energy gap, which act as indirect recombination centers or traps for electrons and holes resulting in photoconductivity in the film. The as prepared sample had a large amount of hydrogen atoms incorporated in it which gave rise to hydrogen related defects and these defects gave rise to localized energy states in the tail regime which could become recombination centers for photoconductivity. Due to significant evolution of hydrogen atoms from the sample annealed at 400°C, dangling bonds formed resulted in localized states or recombination centers in the forbidden gap. These states substantially enhanced the recombination process and thus the photoconductivity as a result of the transition of an electron or a hole from valence band to conduction band or vise versa depending on the energy difference between the state and the conduction and valence band [88].

5.4.2 Effect of Annealing Temperatures on the Activation Energy :

The extended state and the localized state activation energies were calculated from the 1st and 2nd slope of a plot of $\ln\sigma$ versus $\frac{1}{T}$ in the temperature range of 77K-320K. Figure 5.17 shows the effect of annealing temperatures on the activation energy. With the exception of the sample annealed at 100°C, all the samples annealed at temperatures below 400°C exhibited low extended state activation energy (E_C-E_F). This is attributed to high density of states at the mid gap and the tail

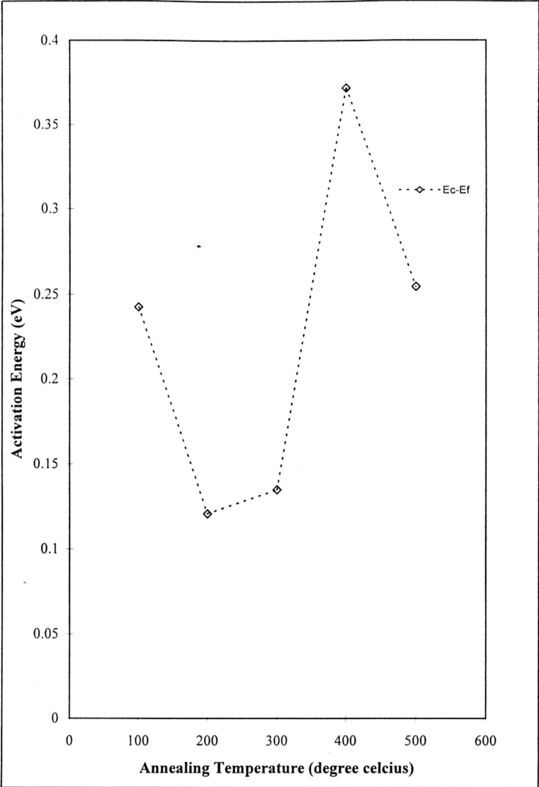

Figure 5.17 The Effect of Annealing temperature on (E_C-E_F).

state region due to deep and shallow defects respectively. The low value of (E_C-E_F) and (E_A-E_F) obtained at these annealing temperatures are due to a competition between extended state and hopping conduction even at temperature close to room temperature. When the sample was annealed at 100°C, the sample exhibited a significant extended state activation energy (E_C-E_F) due to healing of shallow defects or states in the tail state region and the hopping mechanism was confined at low temperature only (<250K). On annealing the sample at 400°C, the shallow defect states were dominant and the film exhibited pure extended state conduction at high temperatures and the hopping conductivity was confined to low temperature only. Thus the film annealed at 400°C showed significant extended state activation energy (E_c-E_F) of 0.37eV. In the case of the sample annealed at 500°C, recrystalization of the film occurred due to high temperature annealing which led to rearrangement of the film structure. The extended state activation energy decreased slightly relative to the sample annealed at 400°C.

5.4.3 Effect of Annealing Temperature and Hydrogen content on the Density of States at the Fermi level:-

Figures 5.18(a) and 5.18(b) shows the effect of annealing on the density of states at the Fermi level and the effect of annealing on the hydrogen content of the sample respectively. Table 5.2 presents the figures for the activation energy and the density of states at the Fermi level. From table 5.2 it is evident that, unrealistic values were obtained for the density of states at the Fermi level $N(E_F)$. Similar observations were also reported by many authors [89,90] or the deviations are attributed to uncertainties in the estimation of σ_0 and T_0 from experimental data [89]. The uncertainties arose because Mott's variable range of hopping implied a large number

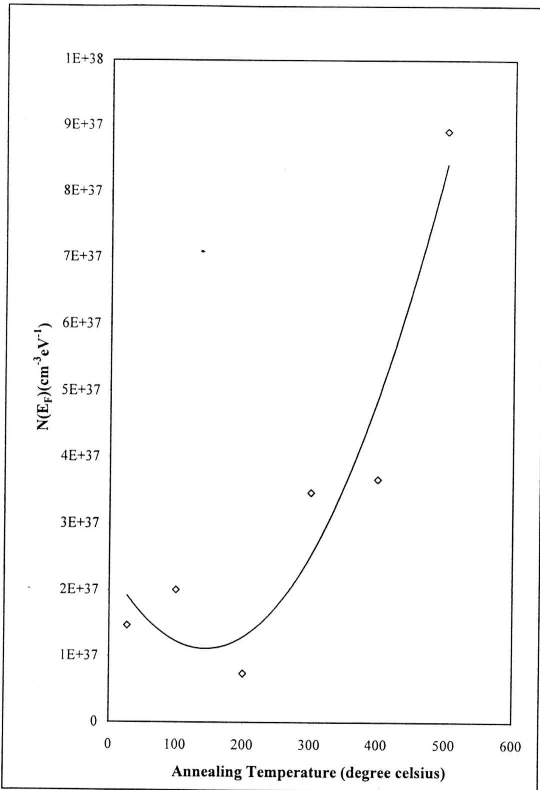

Figure 5.18(a) The effect of AnnealingTemperature on the density of states at the Fermi level

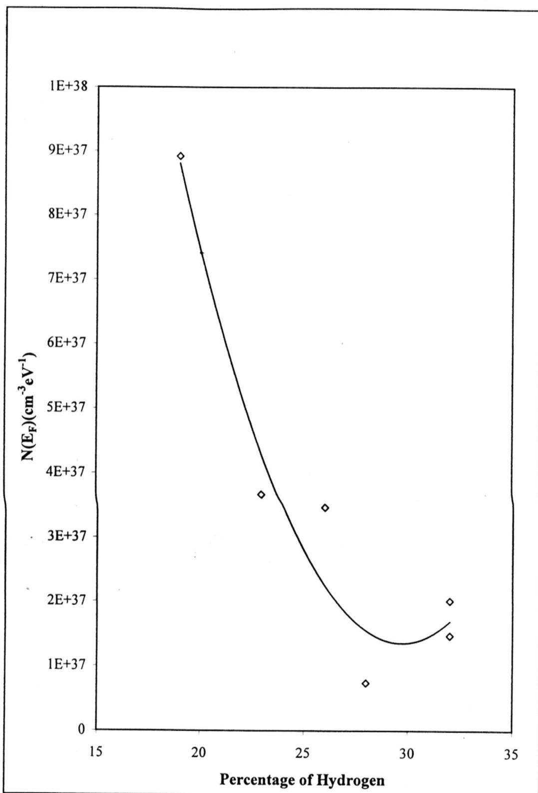

Figure 5.18(b) The Effect of hydrogen content on the density of states at the fermi level

of simplifying assumptions like energy independence of the density of states at E_F, neglection of correlation effects in the tunneling process, Omission of multi-phonon processes and neglection of the electron phonon interaction [91]. However the straight line fit of $\ln\sigma\sqrt{T}$ versus $\frac{1}{T^{\frac{1}{4}}}$ plots at low temperature regime were used as evidence for hopping conduction in the sample and the values of $N(E_F)$ were used to analyze the trend seen in the samples. It is observed from both graphs that the density of states at the Fermi level increases with annealing temperature at annealing temperature above 200°C and decreases with the hydrogen content when the hydrogen content is below 30%. Thus it is evident from both graphs that hydrogen satisfies the dangling bonds and the removal of hydrogen from the structure creates dangling bonds, which forms deep states at the Fermi level. It is also observed from the figure 5.18(a) and (b), the trend is such that $N(E_F)$ decreased with annealing temperatures when annealed at temperatures below 200°C, and $N(E_F)$ increased with hydrogen content when hydrogen content is above 30%. This could be due to the healing process of pure matrix defects on annealing the film at temperature below 200°C and concurrently resulted in reduction in dangling bonds which forms states at the mid gap.

Annealing Temperature (°C)	Thickness of the sample (nm)	Refractive Index (n)	Optical Energy Gap, (eV)	Dispersion energy (E_d)	Oscillation Energy (E_0)	Hydrogen content (% H)	Effective valence electron per anion (N_V)
As Prepared	302	2.39	2.13	26.134	5.726	32	2.066×10^{23}
100	289	2.37	2.17	33.743	6.269	32	3.523×10^{23}
200	269	2.36	2.18	20.352	4.295	28	1.292×10^{23}
300	271	2.35	2.16	36.713	5.383	26	4.271×10^{23}
400	215	2.79	1.82	28.876	4.242	23	1.751×10^{23}
500	223	2.95	1.80	32.109	3.842	19	1.904×10^{23}

Table 5.1 The optical results of the sample annealed at various annealing temperatures

Annealing Temperature (°C)	E_C-E_F (eV)	Density of States at the Fermi level $N(E_F) cm^{-3} eV^{-1}$
As Prepared	0.07	1.47×10^{37}
100	0.24	2.01×10^{37}
200	0.12	7.42×10^{36}
300	0.13	3.47×10^{37}
400	0.37	3.67×10^{37}
500	0.25	8.92×10^{37}

Table 5.2 The Extended state activation energy and the density of states at the Fermi level calculated for the sample annealed at different temperatures